Title: Experience replay facilitates the rapid formation of multi-scale hexagonal patterns of grid cells

Bo Zhang[1,2], Lei Ma[1,3], and Jia Liu[2*]

[1] Beijing Academy of Artificial Intelligence, Beijing, 100084, China

[2] Tsinghua Laboratory of Brain and Intelligence & Department of Psychology, Tsinghua University, Beijing, 100084, China

[3] National Biomedical Imaging Center, College of Future Technology, Peking University, Beijing, 100871, China

*Correspondence shall be addressed to: JL, liujiathu@tsinghua.edu.cn

Abstract

Reverse neuronal replay, characterized by the sequential reactivation of hippocampal place cells to represent past experiences, is proposed to organize learned knowledge into a cognitive map. Here we utilized the continuous attractor model to simulate the formation of multi-scale hexagonal patterns of entorhinal grid cells, which serve as the metric for the cognitive map, during experience replay of hippocampal place cells. We found a significant increase in grid periodicity with reverse replay compared to that without replay. This effect was exclusive to reverse replay, as neither forward nor shuffled-experience replay produced a similar enhancement. Further analysis revealed that the effect of the replay was modulated by the interaction between grid scales and the length of experience replay. That is, the replay was particularly effective for small grid scales, which helped in maintaining the excitation of formed grid bumps during pattern translation. In summary, our study illustrates a causative link between experience replay and the rapid formation of multi-scale hexagonal patterns from computational perspective, providing insights into how the experience replay by hippocampal place cells influences the formation of hexagonal patterns of entorhinal grid cells.

Keywords: neuronal replay, grid cell, Hippocampus, Entorhinal Cortex, continuous attractor model

Introduction

Episodic memory, closely associated with the hippocampus (HPC; Tulving and Markowitsch, 1998; Burgess et al., 2002), is metaphorically characterized as mental travel on a cognitive map (Tolman, 1948; Moser et al., 2017). The travel is guided by hippocampal replay for recollection of the past and anticipation of the future (Fig.1a & b; Foster and Wilson, 2006; Diba and Buzsáki, 2007; Schacter et al., 2007; Carr et al., 2011; Mattar and Daw, 2018; Pfeiffer, 2020). The relational structure of these episodes, fundamental to the mental travel (Hafting et al., 2005; McNaughton et al., 2006; Behrens et al., 2018), is presumably organized by the hexagonal metric of entorhinal grid cells (Fig.1a, c, d; Bellmund et al., 2019; Bellmund et al., 2020; Peer et al., 2021; Whittington et al., 2022), where each episode on the hexagonal metric is represented by the positional coding of multiple grid scales (Fiete et al., 2008; Bush et al., 2015; Stemmler et al., 2015; Bicanski and Burgess, 2019). However, the mechanism through which hippocampal neuronal replay and entorhinal grid metric work together to enable episodic memory remains unclear.

Accumulated evidence suggests that multiple grid scales play a critical role in encoding episodic memory. Anatomically, the spatial scale of entorhinal grid cells is known to increase along the anteroposterior axis, where fine-grained experiences are represented in the posterior area, while coarse experiences are encoded in the anterior area (Hafting et al., 2005; Stensola et al., 2012). Functionally, a scale-dependent functional separation of grid cells are observed in modulating responses to novel versus familiar experiences (Barry et al., 2012). Previous studies suggest that the formation of hexagonal patterns of entorhinal grid cells may be influenced by the experience replay of hippocampal place cells. This is evidenced by reversed reactivations of hippocampal place cell representing unique object sequence structures (Wu and Foster, 2014; Liu et al., 2019; Liu et al., 2021) and the deficits in structured representations resulting from impaired hippocampal replay as reported in both humans with schizophrenia (Nour et al., 2021) and rodent models (Suh et al., 2013). Furthermore, experience replay is detected immediately after linear-track movements lasting less than 10 seconds (Pfeiffer, 2020) and following the first lap of a U-shaped track (Foster & Wilson 2006), aligning with the rapid formation of hexagonal patterns of grid cells (Nau et al., 2018; Killian & Buffalo, 2018; Staudigl et al., 2018; Julian et al., 2018; Wilming et al., 2018).

To establish a causative link between experience replay and the formation of multi-scale hexagonal patterns, here we selectively manipulated the experience replay (e.g., intentionally

turning activating or deactivating it), an endeavor that proves challenging in empirical studies. Specifically, we utilized the continuous attractor network (CAN), also known as the spin-glass model (Fuhs and Touretzky, 2006), which is a well-known model to dynamically elucidate the formation of hexagonal patterns (Burak and Fiete, 2009; Couey et al., 2013; Kang and Balasubramanian, 2019). We used this model to illustrate how the regularity of hexagonal patterns changes as a function of experience replay.

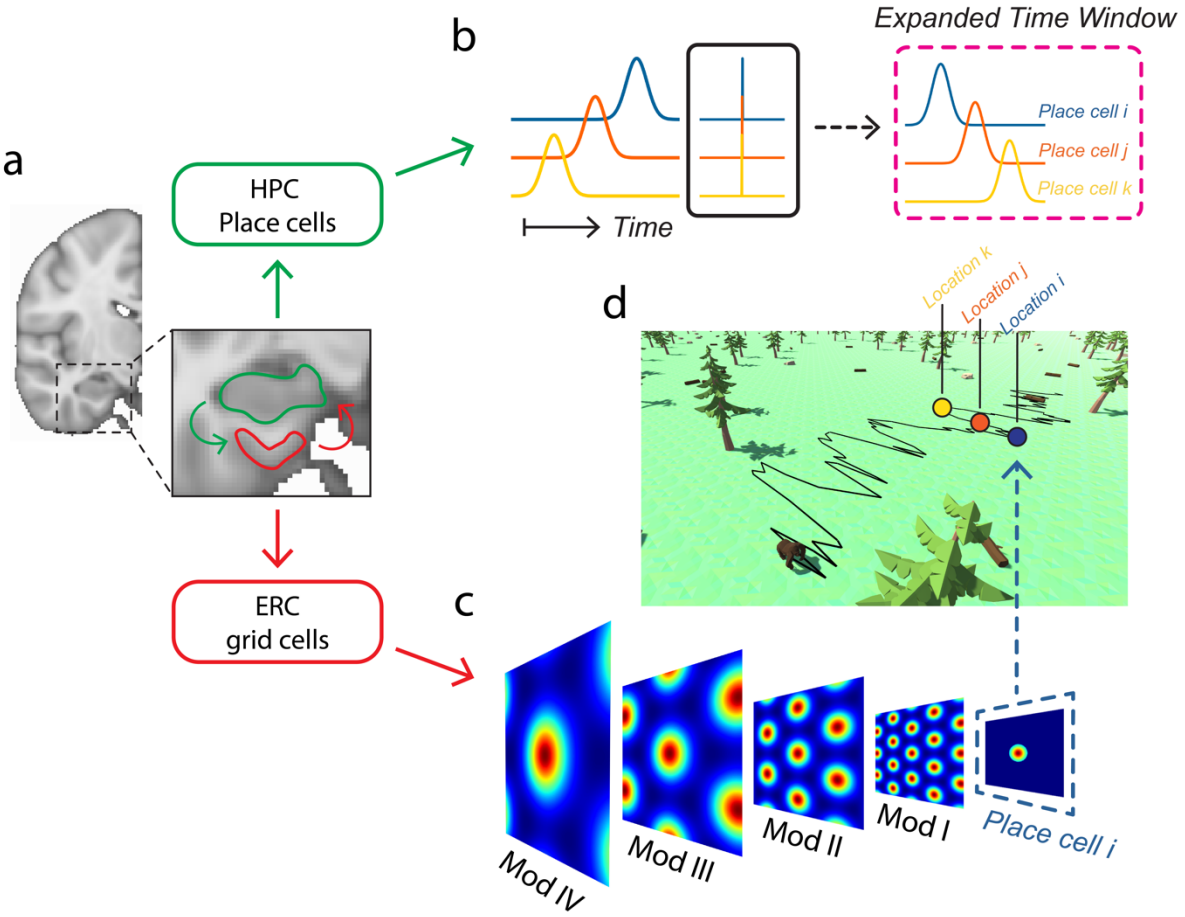

Figure 1. Framework of the recurrent connection between the HPC and ERC. (b) Schema of reverse replay of hippocampal place cells (Foster and Wilson, 2006; Diba and Buzsáki, 2007; Schacter et al., 2007; Carr et al., 2011). Colored lines represent the activity of place cells in temporal domain. Those place cells reactivate in a reversed temporal order (i-j-k) relative to experiences (k-j-i) at the pause location (the blue point shown in d). (c) An example of entorhinal grid cells with multiple scales connecting to place cell for location i (Solstad et al., 2006; Rolls et al., 2006; Bush et al., 2015). Those grid cells are activated by the place cell i (the blue line shown in b and the blue point shown in d) during CAN simulation. (d) A virtual novel environment for illustration purpose, where a gorilla is

designated as an agent, whose trajectory is projected to virtual environment from CAN simulation on a 45-by-45-pixel space.

Results

To examine the effect of reverse replay on hexagonal pattern formation, CAN model was built to translate the excitation-inhibition dynamic of entorhinal grid cells in 45-by-45-pixel neural sheets with the activity at each location representing the response of a hippocampal place cell. Four grid scales were initially designed according to the suggestion of previous studies (Fig.1c, scale [i.e., Mod] I, II, III, and IV; Fiete et al., 2008; Stemmler et al., 2015; Bush et al., 2015). A symmetric excitation-inhibition weight of CAN was made by integrating the two-dimensional representations of the head direction ranged from 0° to 360° radiating from that location (Fig.S4; Fuhs and Touretzky, 2006). The model accepts three predetermined allocentric directions (i.e., 70°, 115°, or 160° with 0° pointing towards East) as input (Fig.2a), forming the "walking" experience during the pattern translation. The restriction on movement directions was intentionally used to probe the rapid formation of hexagonal grid signals from eye movements (Nau et al., 2018; Killian & Buffalo, 2018; Staudigl et al., 2018; Julian et al., 2018; Wilming et al., 2018) as compared to a full exploration of the environment (Hafting et al., 2005; Kang and Balasubramanian, 2019). In each direction, the "walking" experience was constituted by either 5, 10, or 15 footsteps with the ending footsteps arranged as pause location for mimicking animal's decision point, where the reverse replay of the immediate past experience occurs to translate dynamics of neural sheets in reverse direction relative to actual experience before the movements of next direction (Foster & Wilson, 2006; Ambrose et al., 2016; Gillespie et al., 2021). The spatial regularity of hexagonal patterns, indexed by Grid-score, was assessed after 15 independent simulations of CAN with the temporal order of three movement directions randomized.

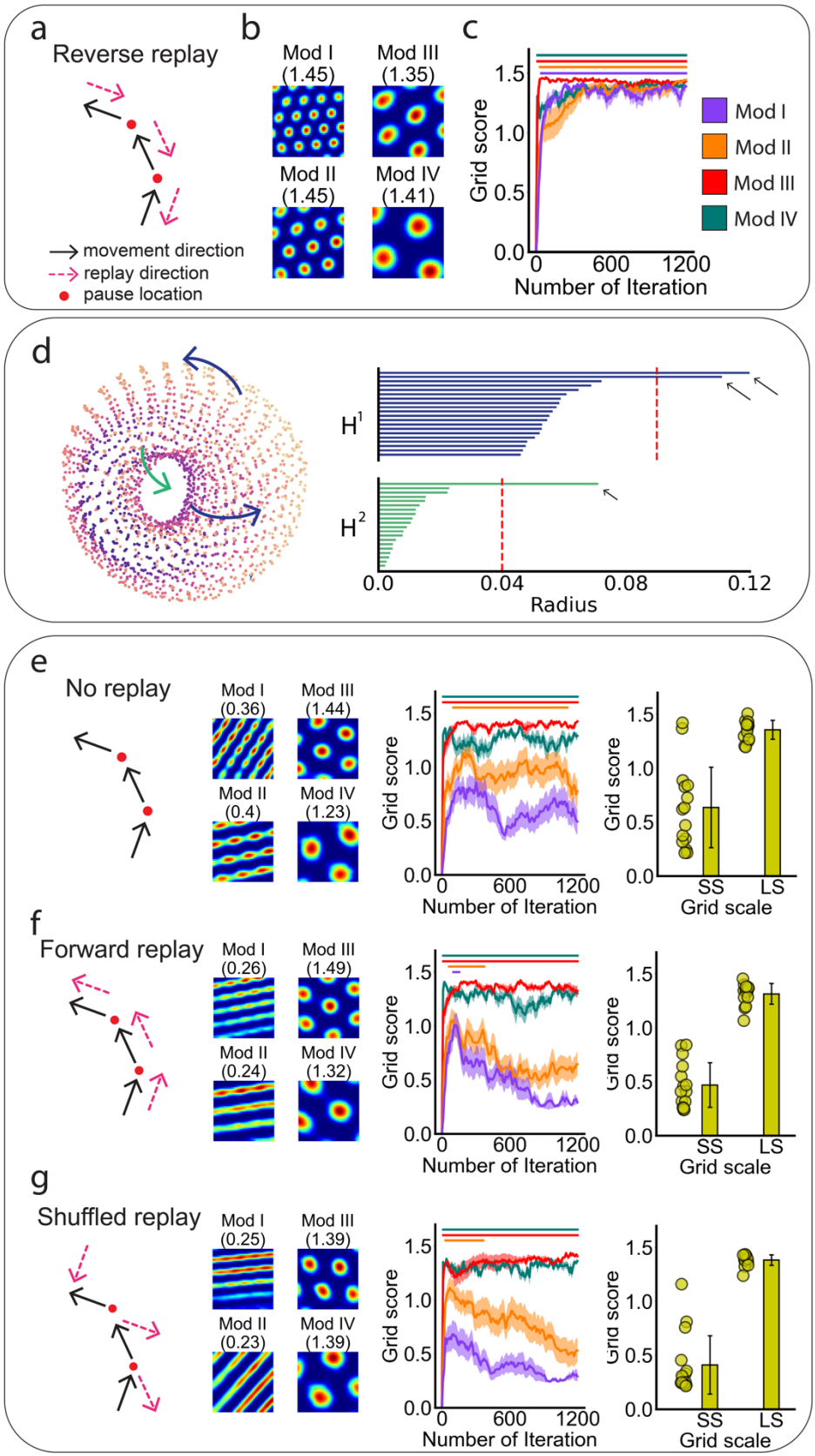
a
Reverse replay
movement direction
replay direction
pause location
b
Mod I (1.45)
Mod III (1.35)
Mod II (1.45)
Mod IV (1.41)
c
Grid score
Number of Iteration
Mod I
Mod II
Mod III
Mod IV
d
H1
H2
Radius
e
No replay
Mod I (0.36)
Mod III (1.44)
Mod II (0.4)
Mod IV (1.23)
Grid score
Number of Iteration
Grid scale
SS
LS
f
Forward replay
Mod I (0.26)
Mod III (1.49)
Mod II (0.24)
Mod IV (1.32)
g
Shuffled replay
Mod I (0.25)
Mod III (1.39)
Mod II (0.23)
Mod IV (1.39)

102

Figure 2. Effect of experience replay on the formation of multi-scale grid cells during limited exploration. (a) Schematic representation of animal movement trajectories. Black arrows denote the movement direction of animal, and red arrows denote the replay direction. (b) An example of the multi-scale hexagonal patterns of grid cell generated by CAN with reverse replay. Values in the brackets indicate Grid-score. (c) Grid-score, averaged across grid cell population in each scale and 15 independent simulations, increased as a function of the number of model iterations. Solid lines above the developmental trajectories indicate that Grid-score reached significance ($p < 0.05$, initial threshold, $p < 0.05$; corrected for multiple comparisons), and error bars denote standard error. (d) A torus-like structure, derived from dimensionality reduction from the population activity of 484 grid cells of Mod IV. Barcodes with the 20 longest lifetimes from persistent cohomology analysis are shown for the 1D hole (H^1, blue) and 2D hole (H^2, green). The red dashed line indicates the threshold of significance corrected for multiple comparison (radius = 0.083 / 0.024 for H^1 / H^2, respectively). (e)-(g) Examples of the multi-scale hexagonal patterns of grid cell generated by CAN with either no replay (e), forward replay (f), or shuffled-experience replay (g), respectively. The bar charts show the overall Grid-score across four scales, and a dot denotes the averaged Grid-score from one simulation. Note that all models underwent same number of iterations. SS (Mod I & II) and LS (Mod III and IV) denotes small- and large-scale, respectively.

Regular hexagonal patterns emerged for all grid scales at single neuron level, accompanied by a rapid increase in spatial periodicity at the beginning of simulations (Fig.2b & c & Fig.S2a, mean Grid-score of Mod I / Mod II / Mod III / IV = 1.39 / 1.44 / 1.43 / 1.39, respectively; $p<0.05$, initial threshold, $p < 0.05$; corrected for multiple comparisons). Next, we examined the spatial periodicity of grid cells at population level by following the procedure of toroidal topology detection (Gardner et al., 2022). The joint activity of rats' grid cells resides on a toroidal manifold as expected by the twisted torus model (Samsonovich and McNaughton, 1997). As the result, we observed the toroidal structure from the population activity of 1936 grid cells (Fig.2d & Fig.S3; i.e., 484 grid cells for each scale, see Method for details), as indicated by the significant lifetimes of barcodes for two one-dimensional holes (the blue arrows, representing the inner and outer hole of the torus) and one two-dimensional hole (the green arrow, indicating the cavity within the torus). Those results confirmed that, with the application of reverse replay, multi-scale hexagonal patterns were successfully formed by the CAN model, despite constrained environmental exploration.

To examine the necessity of reverse replay, three control simulations were performed. First, we examined the effect of replay using a no-replay simulation where only the actual experience was applied to the model. Interestingly, deficits in grid periodicity were revealed particularly for grid Mod I & II (Fig.2e & Fig.S2a, mean Grid-score of Mod I / Mod II = 0.49 / 0.77), where grid periodicity showed a transient increase from the beginning, followed by a sharp decrease to yield a stripe pattern (Yang et al., 2004). In contrast, grid periodicity was observed for large-scale (LS, Mod III & IV, mean Grid-score of Mod I / Mod II = 1.42 / 1.29; $p<0.05$, initial threshold, $p < 0.05$; corrected for multiple comparisons). Second, we examined the direction-dependency of replay by applying forward replay, which is hypothesized for predicting future (Carr et al., 2011; Pfeiffer, 2020), wherein the location sequence was sent to the model preceding the actual experience. This manipulation resulted in a similar pattern with the no-replay simulation (Fig.2f & Fig.S2a, mean Grid-score of Mod I / Mod II = 0.29 / 0.64; mean Grid-score of Mod III & IV = 1.32 / 1.30; $p < 0.05$, initial threshold, $p < 0.05$; corrected for multiple comparisons). Third, we examined the role of the relational structure of reverse replay by shuffling the order of experiences. Again, scrambling the spatial-temporal structure of reverse replay significantly reduced the Grid-score in grid Mod I & Mod II (Fig.2g & Fig.S2a, mean Grid-score of Mod I / Mod II 0.29 / 0.53) and had

little effect on grid Mod III & Mode IV (mean Grid-score of Mod III / Mod IV = 1.40 / 1.36; $p < 0.05$, initial threshold, $p < 0.05$; corrected for multiple comparisons).

Taken together, these findings suggest that reverse replay, which offers a sequential structure opposite to actual experience, is significantly more effective for the formation of hexagonal patterns in small scales than in large scales. No effect was observed with no replay, forward replay, or shuffled-experience replay (fig.2e-g right; Mod I & II versus Mod III & IV: $t(14) = 7.02 / 13.89 / 13.28$ for no replay, forward replay, and shuffled-experience replay, respectively, $p < 0.001$, two-sided), suggesting the necessity of reversed replay in constructing a high-resolution cognitive map.

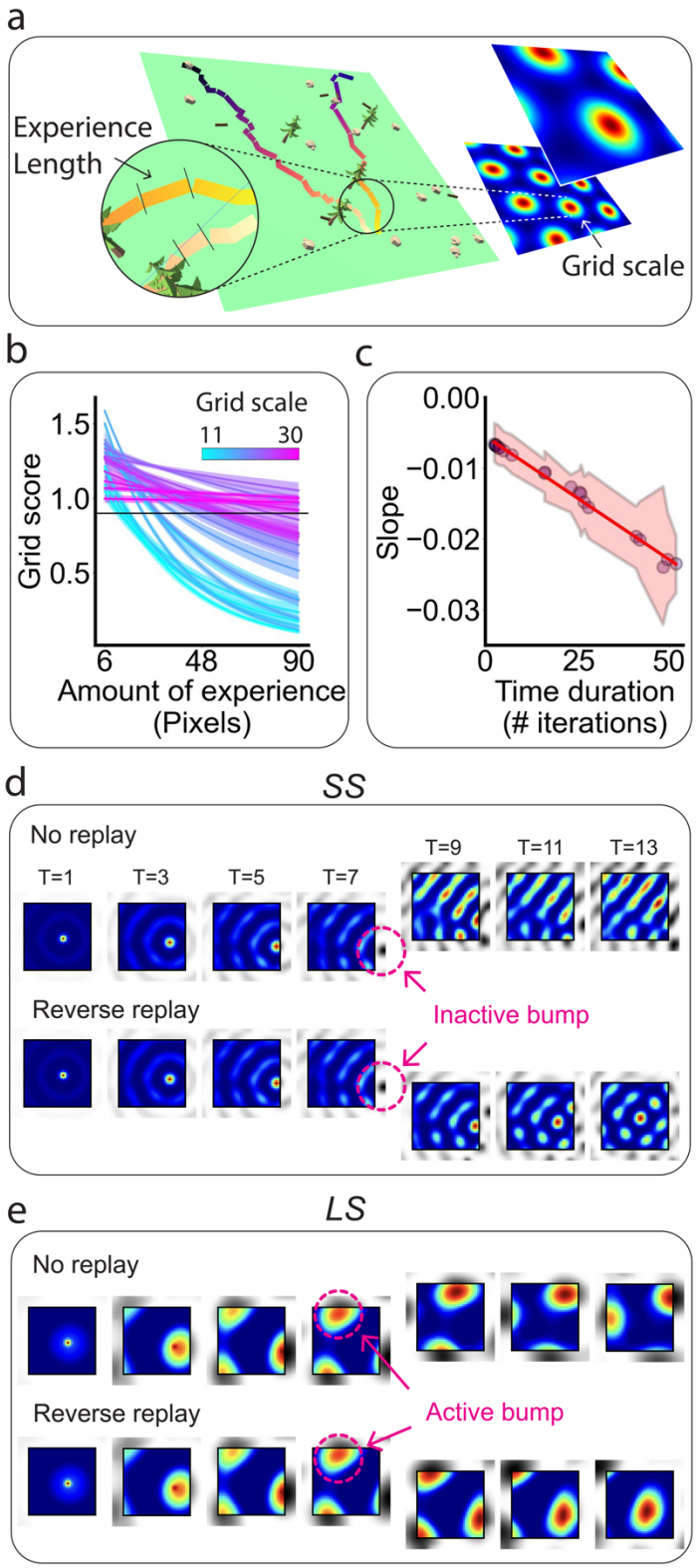

Figure 3. Mechanism of reverse replay on hexagonal pattern formation. (a) Schematic diagram that illustrates the manipulation of experience-length and grid scale in the simulation. (b) Grid-score changes, represented as a function of experience-length and grid scale, are fitted by an exponential decay function (R^2=0.62, P<.0.001). (c) The

interaction of experience-length and grid scale, indexed by the slope (i.e., decay rate), predicted the temporal dynamics of hexagonal pattern formation during iterations (R^2=99.3%, P<0.001). (d) & (e) Two representative cases that illustrate how reverse replay influences grid periodicity, particularly in the case of small-scale (SS). In the SS case (d), after the rapid formation of periodicity during T1-5, the immediate recall (i.e., reverse replay) maintained the excitation of the already-constructed bump by propagating it back to the space during T9-13. This process effectively prevented the disruption of a grid-like pattern to a stripe-like pattern. In contrast, in the LS case (e), there was an earlier formation (T3-5) of grid periodicity than the SS case (T7-9). Specifically, the newly constructed bumps in T7 played a role in excitation-inhibition dynamics, which prevented the disruption of spatial structure even though the earlier generated bump propagated out of the space.

Why experience replay selectively promoted the formation of hexagonal pattern with small scale? To address this question, we explored the mechanism of the interaction between experience replay and grid scale on the formation of hexagonal patterns. Specifically, we asked how the regularity of hexagonal pattern changed as a function of the length of past experience (LPE), indexed by the number of footsteps in a single episode (Fig.3a, Left), and the wavelengths of the grid pattern (WGP), indexed by grid scales (Fig.3a, Right). Accordingly, we simulated models with 12 pairs of LPE and WGP parameters (see Table.S1, and Methods for details), respectively, and examined how Grid-score changed as a function of LPE and WGP.

As expected, we observed a significant main effect of LPE ($F(1,576) = 499.8$, $P < 0.001$) and WGP ($F(1,576) = 556.6$, $P < 0.001$) (Fig.S6), suggesting better spatial periodicity with more immediate recall (i.e., shorter LPE) and with larger scales of grid cells (i.e., larger WGP), respectively. Interestingly, the decay rate in spatial periodicity along LPE, indexed by decay slope k (see Methods for details), varied as a function of WGP. That is, smaller scales of grid cells were associated with a faster decay rate, where decay slope k strongly correlated with grid cell scales ($R^2 = 0.62$, $P < 0.001$). This observation was further confirmed by a significant modulation effect of WGP when the replay was applied as opposed to no replay (replay: $F(1,576) = 117.8$, $p < 0.001$; no replay: $F(1,576) = 0.84$, $p = 0.36$). Critically, the slope k, determined under the interaction of LPE and WGP, predicted the time needed to form a grid pattern with a satisfactory Grid-score (Fig.3c & Fig.S7; R^2=99.3%, $P<0.001$). For example, the formation time of grid cells of a smaller scale associated with more immediate recall (i.e., a smaller k) was equivalent to the formation time of grid cells of a larger scale associated with less immediate recall.

This observation thus provides a potential explanation for the role of reverse replay in maintaining the hexagonal patterns. For example, when a small-scale grid cell traverses through space, a grid-like pattern forms quickly (T = 5, Fig.3d, left), showing an initial increase in Grid-score at the development stage (Fig.2). However, the active bump, which preferentially represents the self-location formed by the CAN model (Fig.S4), easily propagates out of the space (T = 7, Fig.3d, middle). In the absence of replay, the grid-like pattern disintegrates into a stripe-like pattern (T = 11, Fig.3d, top right). In contrast, immediate recall (i.e., reverse replay) enables the bump to propagate back into the space, allowing the maintenance and further development of the grid-like pattern (T = 13, Fig.3d, top bottom). On the other hand, a large-scale grid cell not only possesses a larger bump that remains active for a longer duration (T = 7, Fig.3e) but also forms a grid-like

pattern more quickly (Fig.3c & Fig.S7); therefore, a regular grid pattern is formed before the bump becomes inactive. Accordingly, reverse replay is no longer needed for pattern maintenance. Therefore, the effect of reverse replay on grid periodicity depends on the interplay of multiple factors, such as environmental characteristics (e.g., the size and structure of the space), biological properties (e.g., grid scales/WGP, time constant τ of CAN, and the length of past experience/LPE), and actual navigation behaviors (e.g., movement direction).

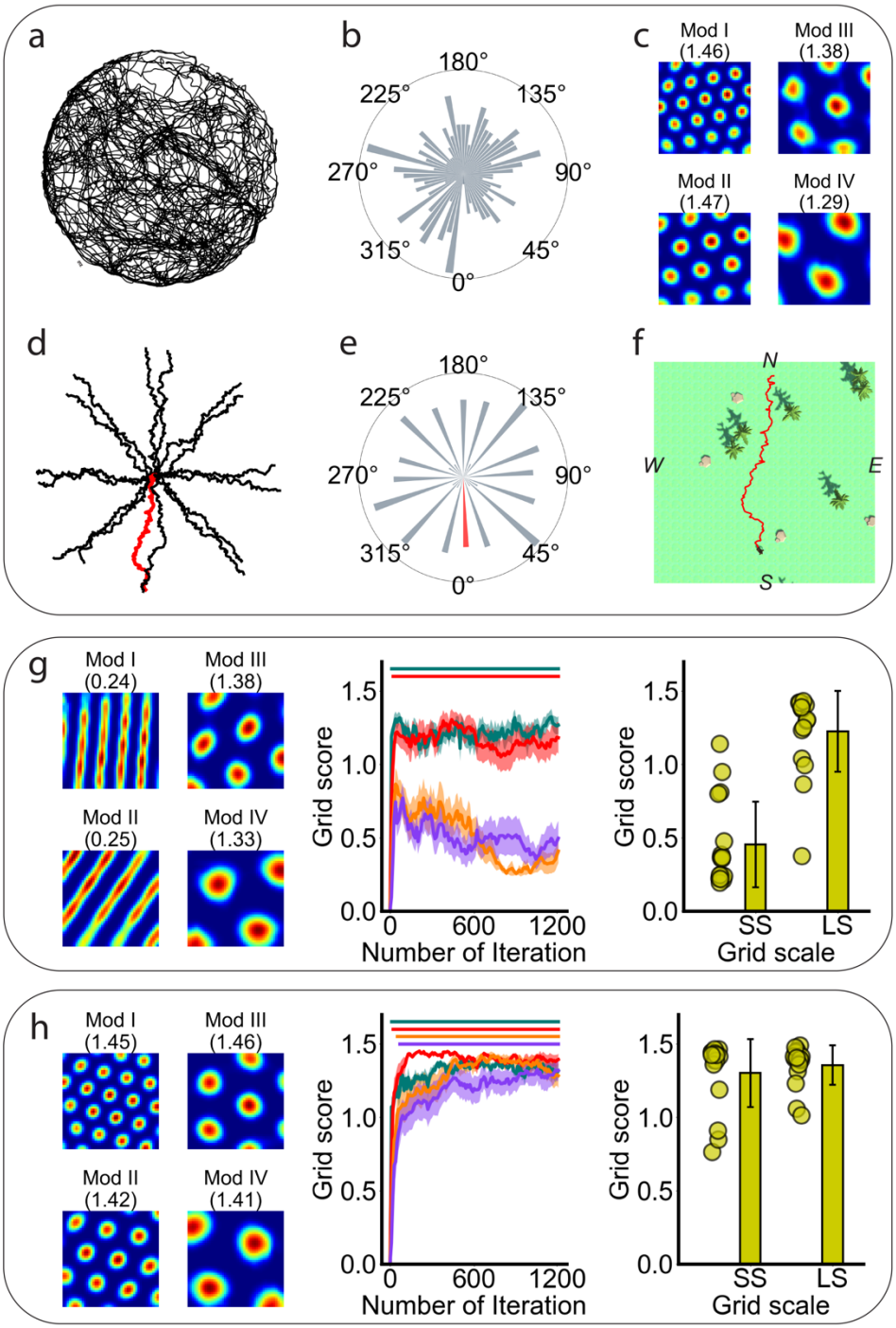

Figure 4. Effect of experience replay on the formation of multi-scale grid cells during extended exploration. (a) Animal trajectories, obtained from open-source data (Hafting et al., 2005), were used as input of CAN, (b) A polar plot denoting the distribution of movement directions, (c) An example of the multi-scale hexagonal patterns of grid cells generated by CAN with animal trajectories as input and no experience replay was applied; Grid-scores are shown in bracket. (d)-(f) Simulated trajectories with movement directions uniformly distributed across 0°-360° as indicated by the Polar plot. Each trajectory was governed by a global direction with noise bounded by -90° - 90°. For example, the

trajectory with a global direction towards South, highlighted in red, was associated to the movement directions of 270° ± 90°. (g)-(h) Examples of the multi-scale activity patterns of grid cell generated by CAN with no reverse replay (g) and reverse replay (g), respectively. Line and bar charts showed averaged Grid-score of four scales across 16 independent simulations (d-e). Note that the same number of iterations were applied to all models.

To clearly demonstrate this point, we predict that even small-scale grid cells do not necessitate reverse replay to form regular hexagonal patterns if their bumps remain active through continuous change in the direction of movement, thus confining the bumps within the space. This is precisely what animals do. An analysis of mouse movement traces (Fig.4a, Hafting et al., 2005) showed that the movement directions were uniformly distributed from 0° to 360° ($p = 0.23$, Rayleigh test, Fig.4b). Furthermore, when we applied the same trace to the virtual gorilla, regular periodicity was observed for all grid scales without the need for replay (Fig.4c, Grid-score= 1.46/1.47/1.38/1.29 for Mod I / II / III / IV, respectively. $p < 0.05$, initial threshold, $p < 0.05$; corrected for multiple comparisons).

To further examine the necessity of this strategy, we designed trajectory traces, each of which aimed towards a global direction with random noise of direction applied at each local location (Fig.4d-f and Fig.S8, $p < 0.001$, Rayleigh test; see Methods for details). In this scenario, the bump of grid cell likely propagates out of the space before the hexagonal pattern forms reliably. Indeed, without replay, we observed a stripe pattern in small-scale grid cells (Fig.4g & Fig.S2b, mean Grid-score of Mod I / Mod II = 0.49 / 0.41, respectively), which had a significantly lower Grid-score than that of large-scale grid cells ($t(15) = 7.47$, $p<0.001$, two-sided). As expected, the irregularity in periodicity was eliminated with reverse replay (Fig.4h & Fig.S2b, mean Grid-score= 1.32 / 1.28 / 1.39 / 1.32, for Mod I / II / III / IV, respectively. $p < 0.05$, initial threshold, $p < 0.05$; corrected for multiple comparisons), significantly more regular than that without replay (Fig.4h, $t(15) = 8.85$, $p<0.001$, two-sided). Considering the habit of animals to randomly change direction while navigating novel environments, reverse replay seems not necessary. However, it becomes critical, especially for small-scale grid cells, when animals need to rapidly form hexagonal patterns of grid cells with limited environmental exploration.

Discussion

This study utilized the CAN model to examine the role of experience replay in facilitating the hexagonal pattern formation of grid cells. We found that reverse replay, as opposed to no replay, forward replay, or shuffled-experience replay, significantly enhanced grid periodicity. Specifically, experience replay was particularly effective in enhancing the spatial periodicity of small-scale grid cells, thus assisting in the construction high-resolution cognitive map (Schuck and Niv, 2019). Further analyses revealed that the relationship between experience replay and hexagonal pattern formation was modulated by the interplay between the spatial scales of grid cells and the length of past experience, which ensured that the active bumps were not disrupted by wave propagation by balancing between the size of grid scale and the duration of past experience. In summary, our results revealed a causative relationship between experience replay and hexagonal pattern formation from a computational perspective. This revelation may provide insights into how reverse reactivations of hippocampal place cell construct abstract knowledge structures by facilitating the hexagonal pattern formation of Entorhinal grid cells (Suh et al., 2013; Wu and Foster, 2014; Liu et al., 2019; Nour et al., 2021; Hafting et al., 2005; McNaughton et al., 2006; Behrens et al., 2018).

One distinct advantage of computational modelling is to allow for careful and intentional manipulation of all parameters. In this study, we utilized the CAN model to simulate the excitation-inhibition dynamics of grid cells (Burak and Fiete, 2009; Couey et al., 2013; Shipston-Sharman et al., 2016; Kang and Balasubramanian, 2019; Khona & Fiete, 2022) and revealed two novel findings. First, under circumstances of limited environment exploration, reverse replay is necessary to form hexagonal patterns of small-scale grid cells, highlighting the potential of reverse replay to quickly and flexibly form hexagonal patterns without the need for extensive environmental exploration. This finding may help explain previous findings of grid periodicity in one-dimensional linear virtual track (Yoon et al., 2016) and circular track (Jacob et al., 2019), as well as during rapid visual mapping (Staudigl et al., 2018; Julian et al., 2018). In these irregular environments and task-dependent demands, traditional long-term exploration strategies may be less effective; in contrast, experience replay can provide a rapid and efficient mechanism to adapt to these situations, enabling quick establishment of spatial representations under various constraints.

Second, by systematically manipulating WGP (large versus small scales), LPE (long versus short length of experience), and tasks (free versus limited explorations), we revealed that the effect

of reverse replay on grid periodicity is modulated by interactions of various factors, more complex than originally assumed derived from empirical studies. However, the underlying mechanism remains the same, as the function of reverse replay is to preserve the formed pattern by initiating reverse replay before the active bumps propagate out of space because of wave propagation. Therefore, reverse replay is particularly important for small-scale grid cells because the formation of small-scale hexagonal patterns demands more time and is therefore more susceptible to pattern disruption, suggested by the reaction-diffusion model where Turing instability varied as a function of spatial frequency in pattern formation (Yang et al., 2004).

The distinct dynamics of small and large grid scales dovetail nicely with the multi-scale representation observed in the anterior (ventral) and posterior (dorsal) HPC (Strange et al., 2014; Schiller et al., 2015). The anterior and posterior of the HPC are known to encode coarse-grained and fine-grained experiences, respectively. Specifically, the posterior HPC, the site commonly selected for recording neuronal replay (Bendor & Wilson, 2012; Carr et al., 2012; Gillespie et al., 2021), might be specifically involved in the hexagonal pattern formation of small-scale grid cells with the presence of experience replay. This conjecture is supported by the occurrence of hippocampal sharp wave ripples, which facilitate experience replay and are typically characterized by transient high-frequency oscillations for precise location coding (Buzsáki, 2015; Ambrose et al., 2016).

The present study has a number of limitations. First, our results relied on computational modelling to unveil the impact of reverse replay on the dynamic properties of the CAN model, the findings may not fully capture the hexagonal pattern formation of grid cells and the interplay of hippocampal place cells and entorhinal grid cells in biological brain. Second, previous studies demonstrate the generalizable role of neuronal replay in memory consolidation and retrieval (Carr et al., 2011), learning (Momennejad, 2020), and emotional processing (Rihm & Rasch, 2015); thus, future studies are needed to address the computational principle of how cognitive domain-specific entities are assembled into relational structure in the entorhinal-hippocampal circuitry (Kurth-Nelson et al., 2023). Finally, our CAN simulations on hexagonal pattern formation were driven by predefined pseudorandom movements, rather than self-organized path integration guided by hippocampal goal representation (Ormond & O'Keefe, 2022). Future studies may develop a unified HPC-ERC system, which not only simulate the HPC-to-ERC pathway for generating the

entorhinal metrics but also integrate the ERC-to-HPC pathway to generate hippocampal forward replay and self-location updating (Wu and Foster, 2014; Pfeiffer, 2020).

Data availability

Raw data reported in the present study are available from the corresponding author upon reasonable request.

Code availability

Python and .NET code for grid cell simulation and virtual navigation are available at https://github.com/ZHANGneuro/Hippocampal-replay-facilitates-the-formation-of-entorhinal-grid-cells. Scripts for the analysis reported in the present study are available from the corresponding author upon reasonable request.

Conflict of interest

None declared.

Author Contributions

B.Z. and J.L. conceived the study; B.Z. built the computational model and performed the analysis; L.M. provided valuable advice and assistance; B.Z. and J.L. wrote the paper.

Acknowledgments

We thank Dr. Yunzhe Liu for providing valuable comments on the manuscript. This work was supported by the National Key R&D Program of China (2020AAA0105200), China Postdoctoral Science Foundation (2022M710470), Beijing Municipal Science & Technology Commission & Administrative Commission of Zhongguancun Science Park (Z221100002722012), Tsinghua University Guoqiang Institute (2020GQG1016), and Beijing Academy of Artificial Intelligence (BAAI).

Supplemental Material

"Experience replay facilitates the formation of the hexagonal pattern of grid cells"

Bo Zhang, Lei Ma, and Jia Liu

Methods

<u>Continuous attractor network (CAN)</u>

CAN model (Fuhs and Touretzky, 2006; Burak and Fiete, 2009; Couey et al., 2013; Kang and Balasubramanian, 2019), programmed by Torch (Version 1.13, Python version 3.9), was utilized to simulate the formation of hexagonal pattern of grid cells. For each grid cell, the membrane voltage ξ, defined by a two-dimension matrix of 45-by-45 pixel, was created, the spatial phase of the grid cell was then determined by an initial point-like place response at the location j represented by a place cell (Bonnevie et al., 2013; Rennó-Costa and Tort, 2017). During evolution over time, the model accepts walking direction v as input, the firing pattern of each grid cell are translated through the differential equation (equation 1),

$$\tau \frac{d\xi_i}{dt} = -\xi_i + \sum_j W_{ij} f_j + v_i + \varepsilon \tag{1}$$

where the spatial response of grid cell i was updated by the sum of the firing rates of all potential grid cell j that connected to the grid cell i via the symmetric recurrent weight W_{ij} (Fuhs and Touretzky, 2006), a two-dimensional matrix with the value representing the connection strength of the grid cell i and j (equation 2). The matrix W was predefined by the sum of the potential head directions ranged from 0° to 360° radiating from a given location with each direction represented by a two-dimension planar wave (Fig.S4 & Table.S1). Specifically, a planar wave in certain direction θ is formalized by $\cos(\omega(v_x X + v_y Y))$, where the v_x and v_y, derived by $\cos(\theta)$ and $\sin(\theta)$, determine the direction of the activity gradient $v_x X + v_y Y$ in physical space. The spatial frequency ω is derived from grid scales σ (equation 3). Each scale represents the Euclidean distance between the peaks of two adjacent grid fields. For example, the grid scale $\sigma = 10$ (i.e., 10 pixels) demonstrates a lower spatial resolution in compared to the grid scale with $\sigma = 5$.

$$W_{ij} = \sum_{\theta=0}^{359} \alpha \cos(\omega(v_x X + v_y Y)) \tag{2}$$

$$\omega = 2\pi/\sigma \tag{3}$$

The firing rate f_j (equation 1), that derived from the membrane voltage ξ_j via a nonlinear transfer function (equation 4), was inhibited to 0 if its membrane voltage was not exceeding a threshold η, otherwise f_j was determined by the square root of membrane voltage ξ_j, leading to a connection to grid cell i via W_{ij}. τ and ε denotes a time constant of 10 ms and the gaussian noise in walking direction v used during extended exploration, respectively (equation 1). In each step of evolution, the response pattern of grid cell was translated toward the direction v with a step size of 3 pixels.

$$f_{\mathrm{j}} = \begin{cases} \sqrt{\xi_{\mathrm{j}}} & \xi_{\mathrm{j}} > \eta \\ 0 & \zeta_{\mathrm{j}} \leqslant \eta \end{cases} \tag{4}$$

To avoid the edge effect (Samsonovich and McNaughton, 1997; McNaughton et al., 2006; Knierim and Zhang, 2012; Shipston-Sharman et al., 2016; Hägglund et al., 2019; Monsalve-Mercado and Leibold, 2020; Gardner et al., 2022), we assume that the two-dimension translation pattern of grid cell is embedded by a toroidal structure, where the matrix boundary is periodic so that the neural response of grid cell can be translated to opposite edge of matrix after it reached the edge and propagate out of space. To achieve it (Fig.S5), we first computed the grid orientation from the autocorrelation maps of grid cell in each evolution step (Hafting et al., 2005). Second, given grid orientation and phase (i.e., grid scale), we accessed the potential neural responses for each location on the opposite edge relative to translation direction from six potential coordinates on the three main axis of hexagonal pattern using trigonometric function. Third, the neural response in one of the six coordinates within the matrix was randomly selected to fill the location on the opposite edge.

<u>Grid cell simulation</u>

The effects of experience replay and experience-length (LPE) on the regularity of hexagonal pattern were examined using CAN model. For experience replay, we intentionally manipulated it with either No, Reverse, Forward, or Shuffled experience and applied them to pattern translation at the decision point (denoted by red dots in Fig.2a, e-g), which occurs immediately after a past experience. In no-replay, no additional directional input was applied to model relative to actual movement. In forward/reverse replay, a list of identical/reverse directions were sent to model prior to/next to actual movement, respectively. Shuffled replay, which

examines the necessity in maintaining the sequential structure of past experience, was applying the model with a list of reversed directions, which were shuffled in temporal order relative to actual movement. In all simulations, the model passively accepted pre-defined directions for the purpose of control with the maximum of evolutional steps constrained by 1200. The trajectories of those predefined movements were projected on a 3D squared open environment created by Unity (Unity Technologies, San Francisco) for the purpose of visualization, where tree, tree trunk, and stone randomly placed on a flat grassy ground, a virtual Gorilla was used to act as the agent.

Limited exploration. To examine the possibility of the rapid hexagonal pattern formation suggested from previous studies (Nau et al., 2018; Killian & Buffalo, 2018; Staudigl et al., 2018; Julian et al., 2018; Wilming et al., 2018) during CAN simulation, we constrained the number of movement directions to three with 45° apart (70°,115°, and 160° with 0° pointing towards East). This design excluded the possibility of reverse directions relative to past experience, which have been commonly involved in animal studies (Hafting et al., 2005; Kang and Balasubramanian, 2019). One of the three directions was randomly assigned for each evolutional step, and the LPE was either 5-, 10-, or 15- steps for the direction. A pause location, mimicking animal's decision point, was placed between two consecutive directions (denoted by red dots in Fig.2a, e-g). To ensure the stability of model inference, each type of experience replay was independently simulated 15 times in limited exploration before group-level tests were conducted. To examine the interactive role of LPE and grid scale on Grid-score (how Grid-score changes as a function of LPEs and grid scales) in both No and Reverse replay, we additionally prepared a total of 29 LPEs, ranged from 2 to 30 steps with a step of 1, and a total of 20 grid scales, ranged from 11 to 30 pixels (see Table 1 for details), resulting 1160 experiments with each 15 simulations. To quantify the impact of LPEs and grid scales on the temporal dynamics of hexagonal pattern formation (how fast Grid-score reaches the significance threshold), we measured the slope $-\frac{1}{k}$ of the exponential decay function $ae^{(\frac{-LPE}{k})}$ for each grid scale and type of experience replay. The slopes were first linearized via log transformation and was subsequently fitted by the curve_fit function of scipy package (version 1.9.3).

Extended exploration. The role of reverse replay on the formation of hexagonal patterns was examined by two conditions in extended exploration, both of which were involved with hundreds of directions. One was the CAN simulation with the direction input from the open-source data (Fig.4a; Hafting et al., 2005; https://www.ntnu.edu/kavli/research/grid-cell-data), which

included all possible directions ranged from 0° - 360° for pattern translation. The number of evolutional steps for the open-source dataset was down-sampled to 1200. Second, the CAN simulation that accepted the inputs predefined by one of eight global directions, each 45° apart (Fig.4d; 0°, 45°, 90°, 135°, 180°, 225°, 270°, and 315°). In the latter case, the movement direction at each evolutional step was determined by a global direction plus an additional noise ϵ randomly assigned from a range of -90° to 90°, resulted in an extended experience in directions from 0° to 180° relative to the global direction (Fig.4d & f). Importantly, this design excluded the possibility of experiencing reverse direction during pattern translation. To ensure the stability of model inference, each simulation was independently performed 16 times during extended exploration (Fig.4d; twice for each of eight global directions) before conducting the group-level tests.

<u>Validation of grid periodicity</u>

The spatial periodicity of gird cell, as indicated by Grid-score, was computed by following the procedure reported previously (Sargolini et al., 2006; Barry & Burgess, 2017). Specifically, for each neuron generated by the models, the spatial autocorrelation map was estimated by equation 5, where $\lambda(x, y)$ denote the activity strength at location (x, y), while τ_x and τ_y denote the spatial shifts of the firing pattern from the neuron. With the rotation of autocorrelation map by 30°, 60°, 90°, 120°, and 150°, Grid-scorewas computed as the difference between the lowest correlation of 60° and 120° and the highest correlations of 30°, 90° and 150°.

$$r(\tau_x,\tau_y) = \frac{n\sum\lambda(x,y)\lambda(x-\tau_x,y-\tau_y) - \sum\lambda(x,y)\lambda(x-\tau_x,y-\tau_y)}{\sqrt{n\sum\lambda(x,y)^2(\sum\lambda(x,y))^2}\sqrt{n\sum\lambda(x-\tau_x,y-\tau_y)^2(\sum\lambda(x-\tau_x,y-\tau_y))^2}} \quad (5)$$

For the regularity of grid cell population, we examined the toroidal structure of population activity of grid cells using persistent homology (Ghrist, 2008), which was performed by the package Ripser++ (Version 1.1.2) for GPU acceleration (Zhang et al., 2020; Bauer, 2021). The principle behind persistent homology is to identify the toroidal characteristics from the global topological feature constituted by point-clouds (the firing maps of grid cell) in 3D Euclidean space. Specifically, we followed the outlines published previously (Gardner et al., 2022). At each grid scale, principal component analysis was performed on the population activity of grid cells, then the first six principal components were further dimension-reduced by uniform manifold approximation into 3D projection. In the 3D space, the data points were Z transformed and were

replaced with simplicial complexes. Upon increasing the radius of simplicial complexes, the complexes are gradually connected and form certain global structure. To examine the emergence of toroidal structure, the life spans (the barcodes) of two 1D holes (the inner and outer hole of torus) and one 2D hole (the cavity in the interior of torus) were tracked throughout the duration of holes from it appear to disappear. Assuming that the life time of a given hole were long enough, the hole would be considered to be contained robustly by the global structure of connected complexes.

Statistics

To quantifying the periodicity of firing patterns generated by CAN, the significance threshold was accessed by field-shuffling permutation (Fig.S9; Krupic et al., 2012). The threshold was derived from the models with reverse-replay applied, which produced the most regular hexagonal patterns across grid scales. Specifically, the long-range spatial structure (global structures of firing field) of given firing pattern was disrupted by shuffling the firing fields 100 times with the local structure (single firing field) preserved. The uncorrected threshold was then determined by the 95th percentile of the shuffling distribution. The significant threshold corrected for multiple comparison was further determined by the 95th percentile of the uncorrected-threshold distribution computed from grid cell population. Similar procedure was used for persistent cohomology analysis, in which the initial uncorrected threshold and the corrected threshold was indicated by the 99th and 95th percentile of the barcode distribution from single and population neurons, respectively. The significance thresholds for the toroidal structure of 1D (H1) and 2D hole (H2) were then averaged across grid scales. The effect of experience-length and grid scales on grid periodicity/grid dynamics were quantified using ANOVA/Pearson correlation, respectively. The difference in grid periodicity between small- and large-scales was examined using two sample t-test. All the t-tests used in the present study were two-tailed.

Figure S1. Grid cell population generated by CAN model with experience replay. For each scale, 24 grid cell samples were shown as example and were sorted by phase along the horizontal and vertical axis.

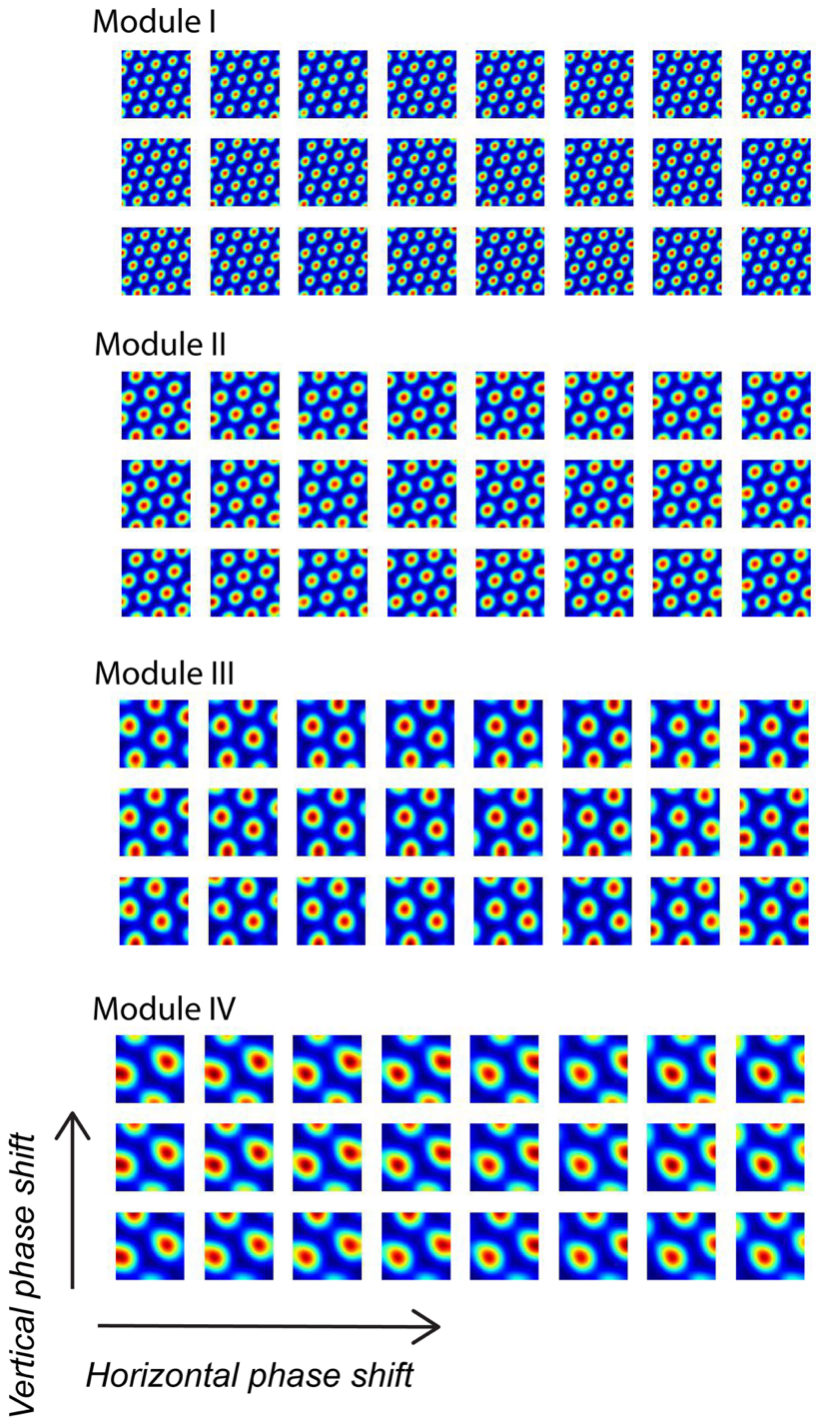

Figure S2. Effect of experience replay on Grid-scores. 15 and 16 independent simulations that correspond to Fig.2 and 4 were performed for (a) and (b), respectively.

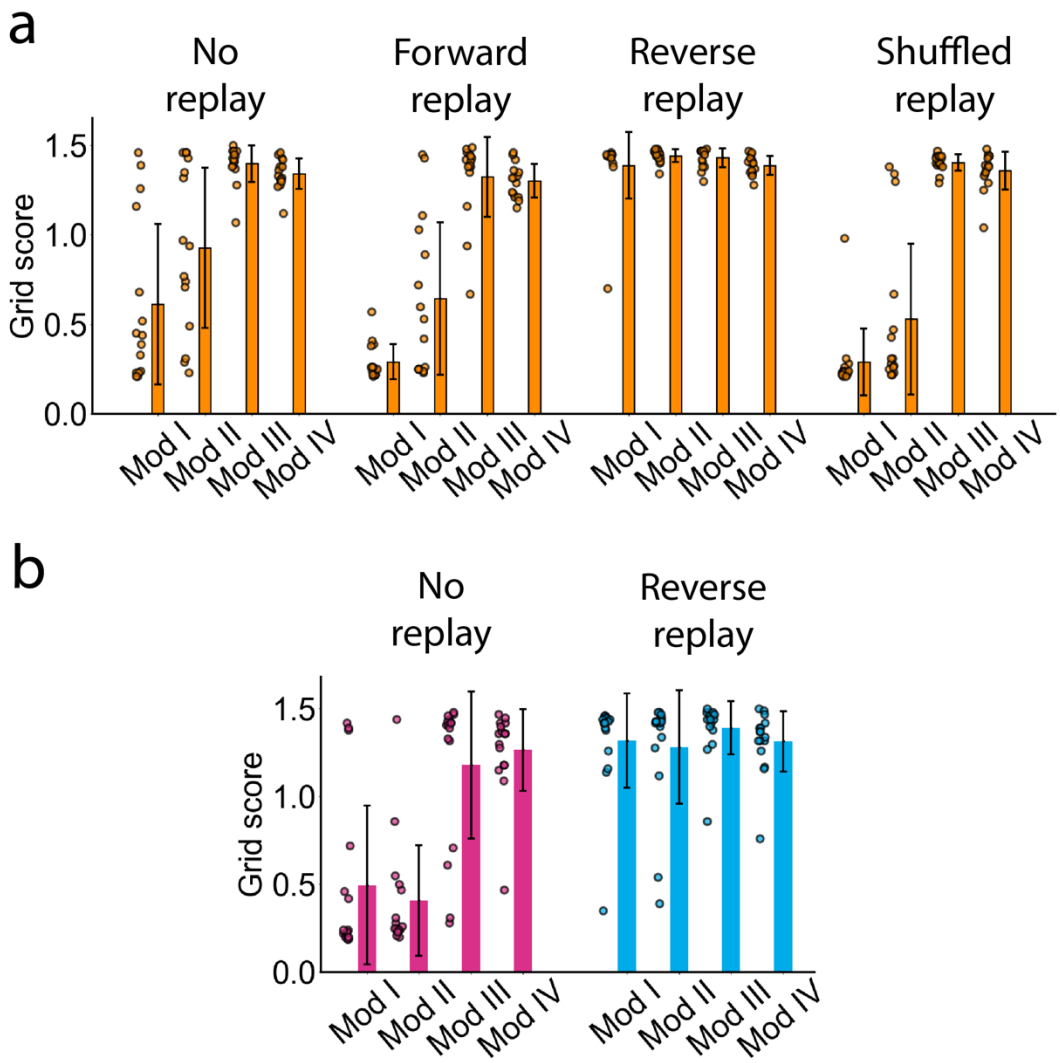

Figure S3. Persistent cohomology analysis on the population activity (484 grid cells) of each grid scale, which were derived from the model with reverse replay applied shown in Fig.2. The barcodes with 20 longest lifetimes were shown for the 1D hole (H1, blue) and 2D hole (H2, green), red dash lines indicate the threshold of significance corrected for multiple comparison.

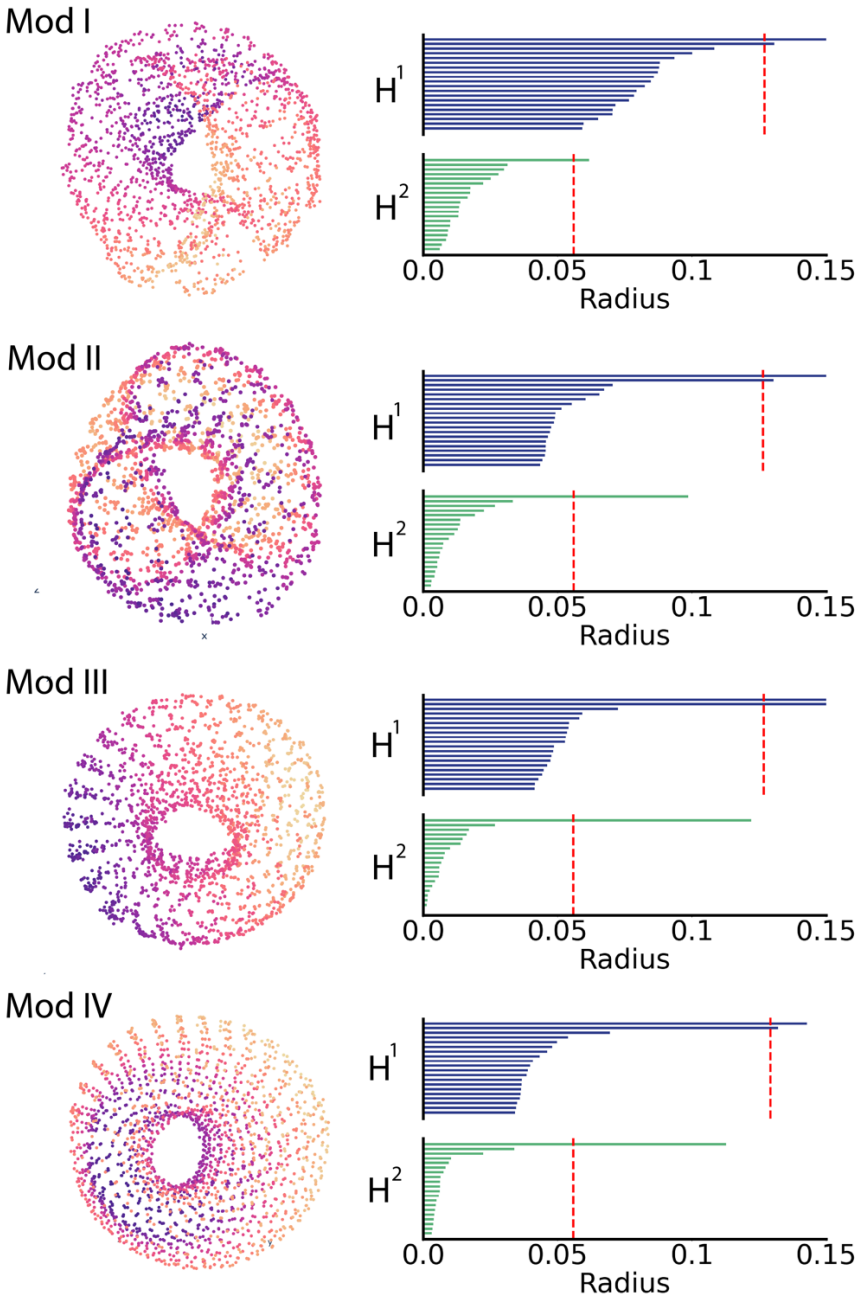

Figure S4. Illustration of the formation of grid cell using CAN model. a) Example of the weight matrix (grid Mod I), which represents the conjunctive head directions of 0° - 360° for a given allocentric location. Each head direction was embedded by a planar wave that represents the unique direction across locations on the two-dimensional space. b) the formation of hexagonal pattern with model iterations (T), regular grid periodicity could be seen by T = 60.

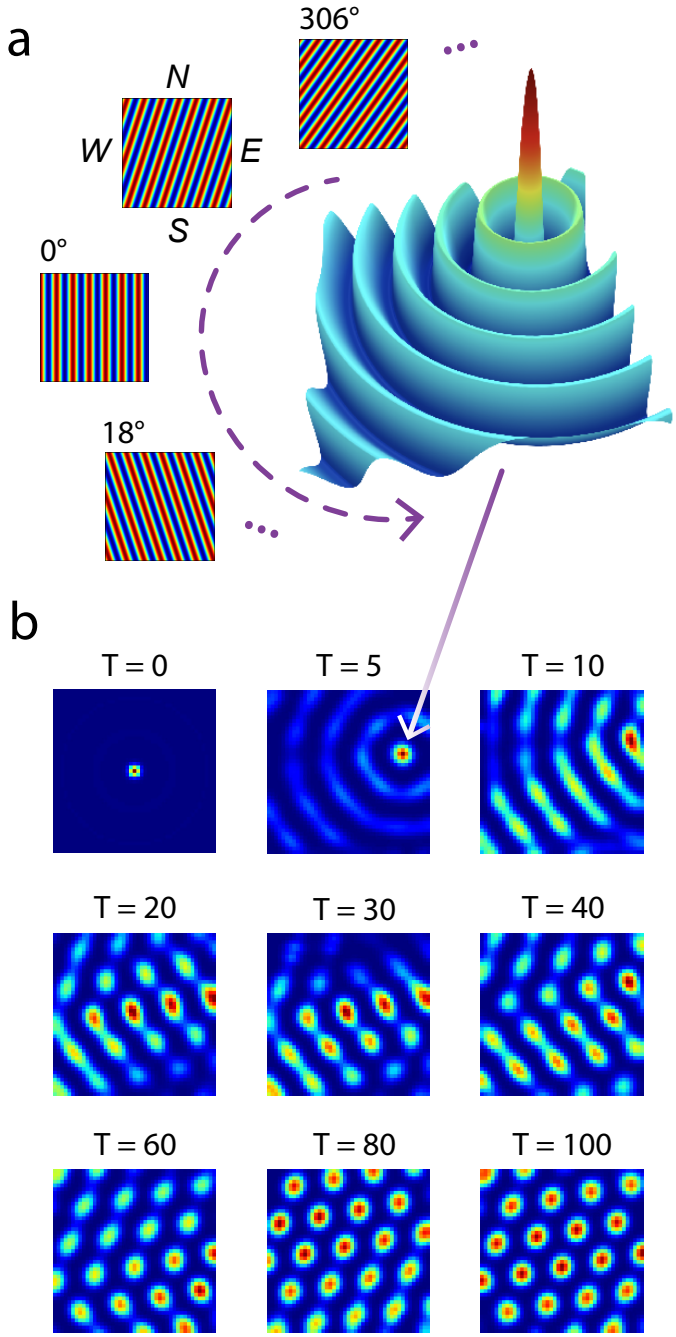

Figure S5. Procedure of interpolation for avoiding edge effect. a) an example of hexagonal pattern, b) grid orientation was computed from the autocorrelation map of original hexagonal pattern, c) the activity at each pixel in the blank area (white color) after a phase shift towards North was assigned from one out of six adjacent locations computed by grid orientation and phase using Trigonometry. d) an example of phase-shifted hexagonal pattern by interpolation.

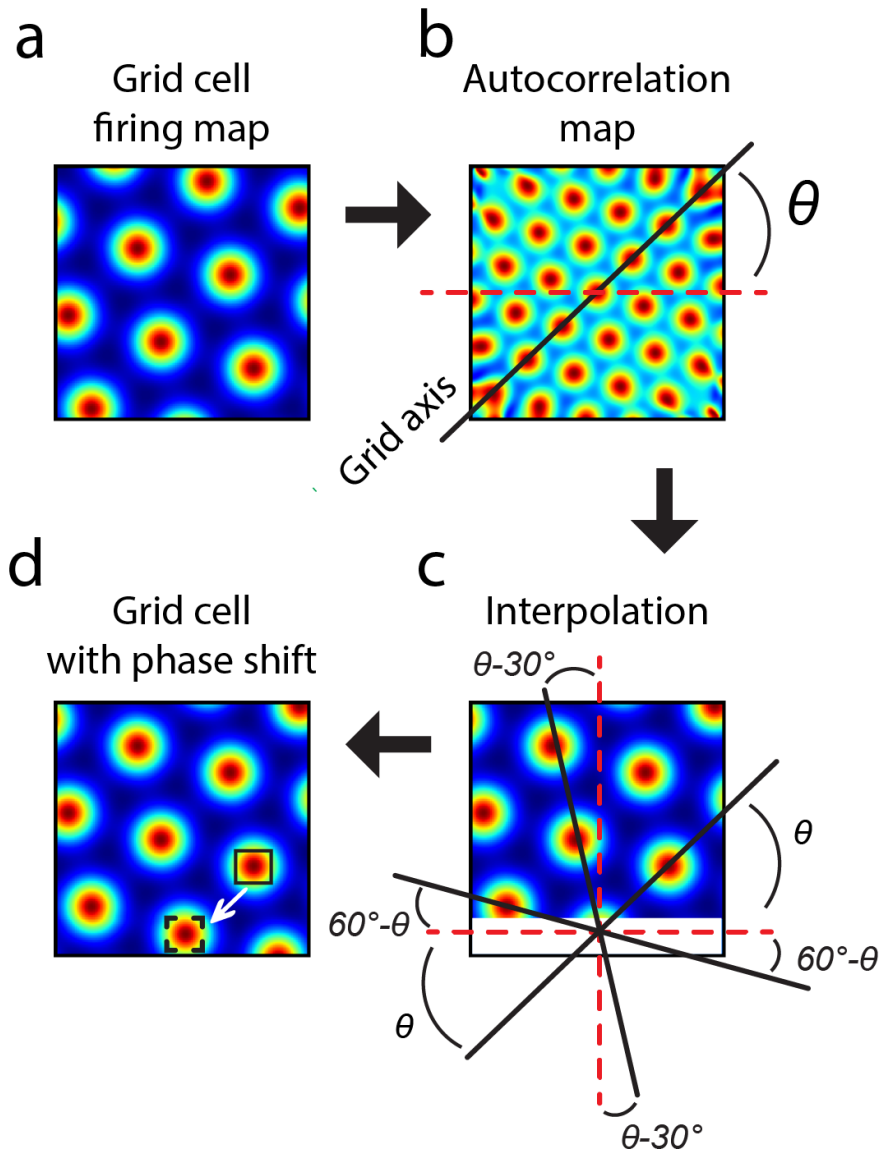

Figure S6. Effect of experience-length and grid scale on grid periodicity. Black/Red line represents the models with no-/reverse-replay applied, respectively. Dashed line indicates the significance threshold of Grid-score. Error bar denotes the standard error of 12 independent simulations.

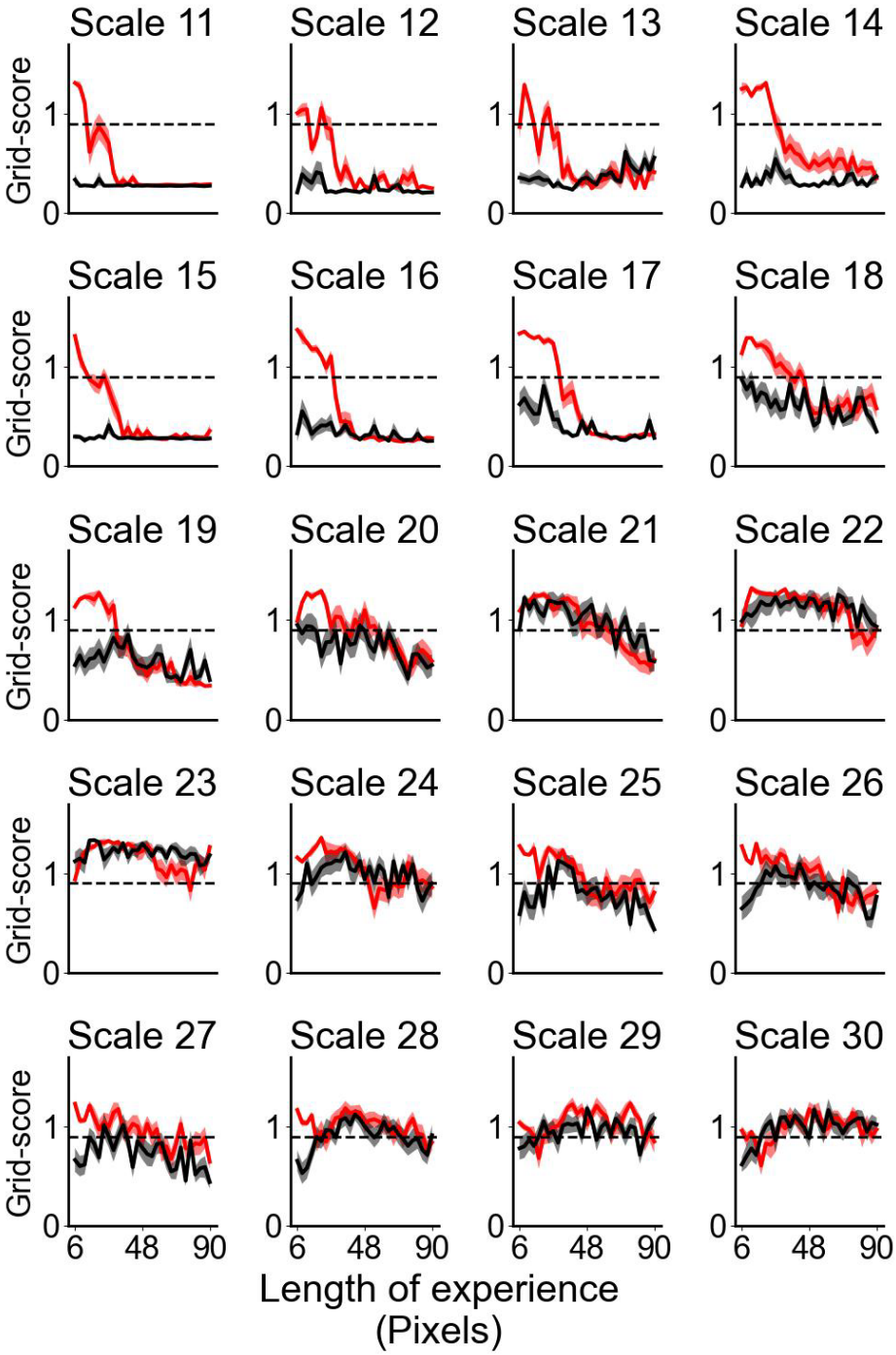

Figure S7. Grid-score changes as a function of iteration. The grid periodicity of large-scale increases faster than the one of small-scale. Red line indicates the iteration where Grid-score reaches the significance threshold. Error bar denotes the standard error of 12 independent simulations.

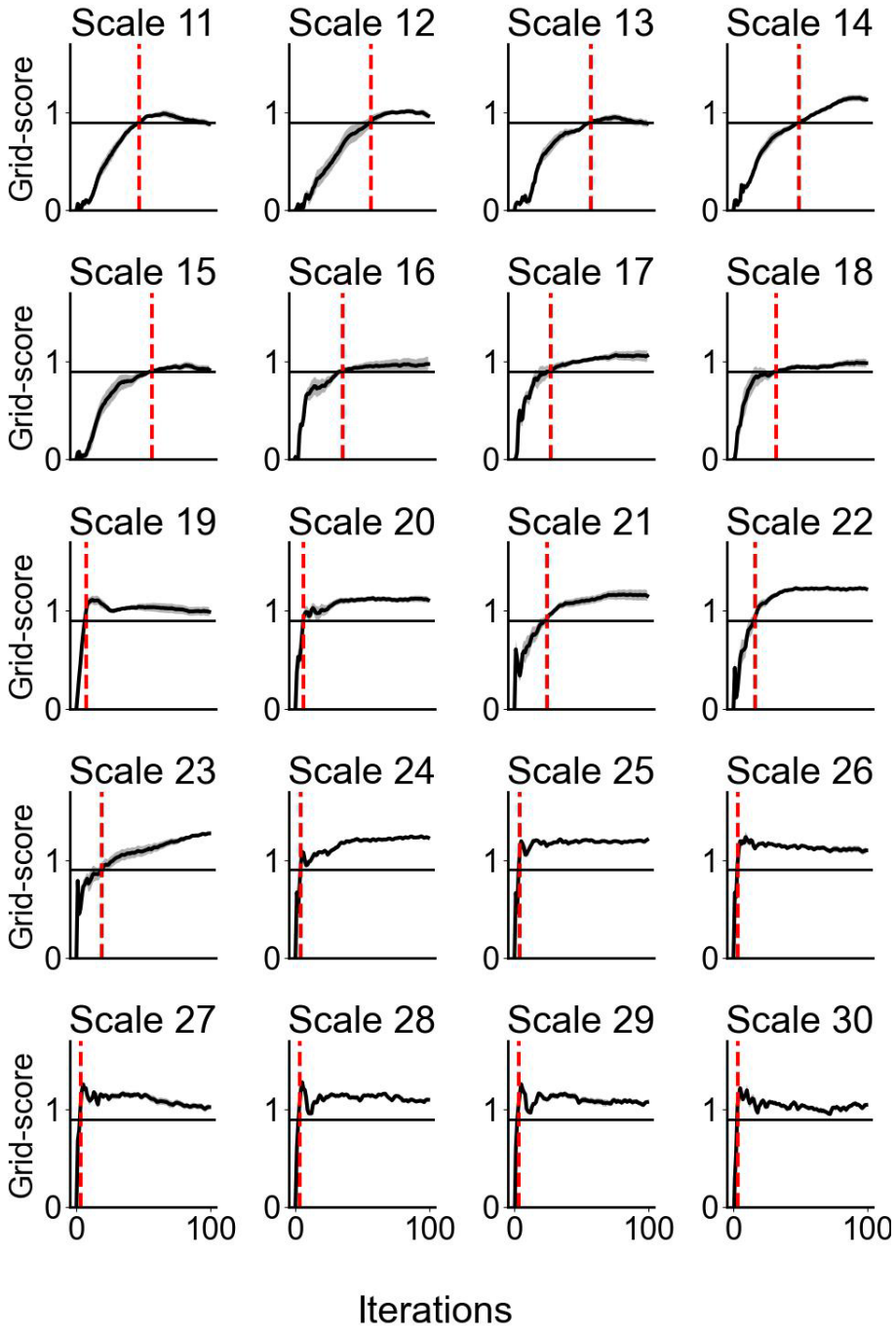

Figure S8. Sixteen independently simulated virtual navigations for each of no-replay and reverse-replay model. Each virtual navigation was dominated by a unique global direction with the noise ranged from -90° to 90° for each footstep. Left column, the distribution of movement directions, black solid line indicates the mean of directions, Right column, Gorilla trajectories during virtual navigation.

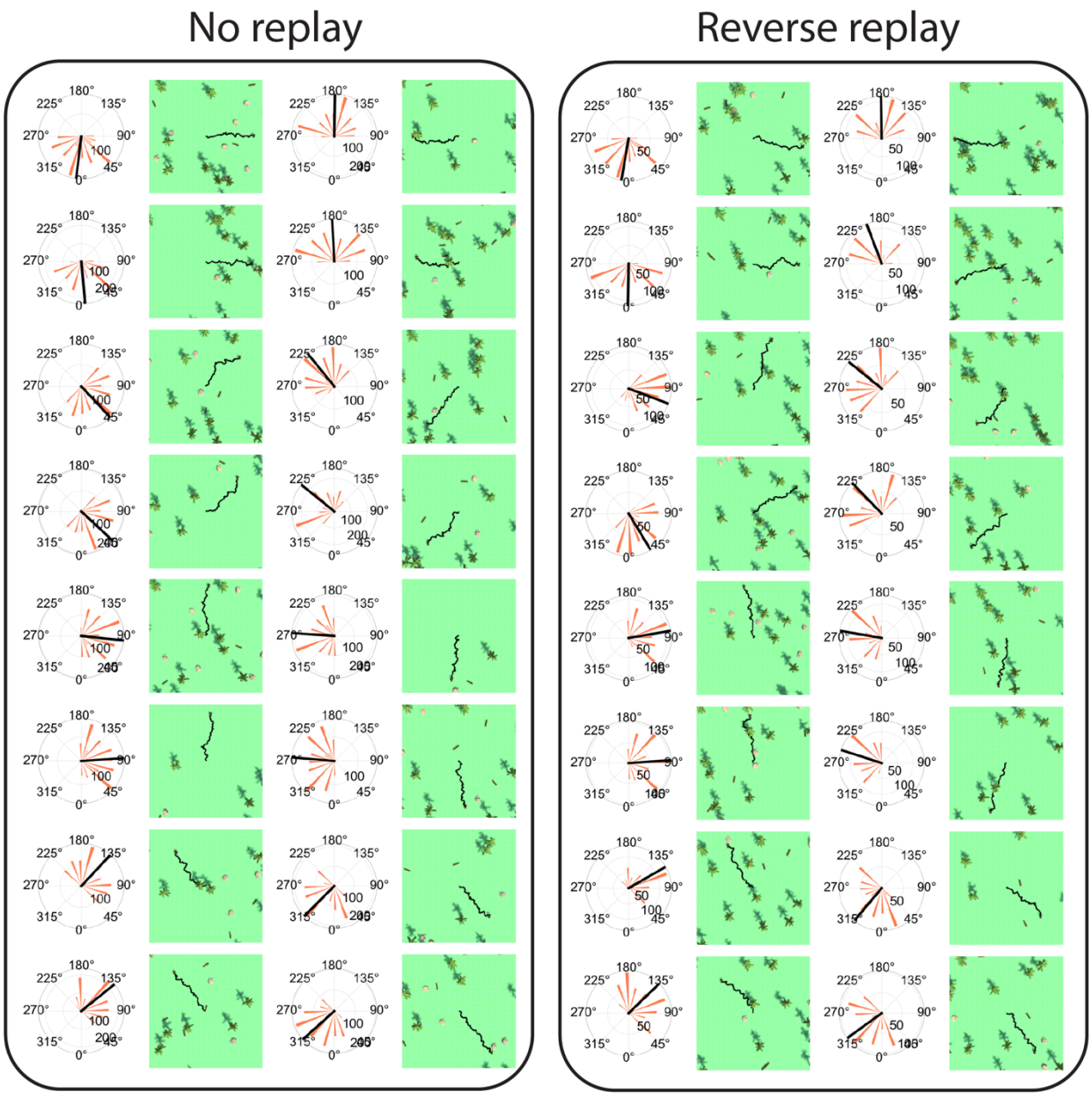

Figure S9. Procedure of field-shuffling permutation. 1) an example of hexagonal pattern, 2) extracting the peaks of the firing field, 3) identifying the local structure of hexagonal pattern, outlined by polygons using Voronoi polygons, 4-5) the firing field that was randomly re-positioned during field-shuffling, (6) the shuffled hexagonal pattern of grid cell, (7) the Grid-score distribution derived from 100 field-shuffling, the black dash line represents the initial (uncorrected) threshold at the 99th percentile of Grid-score distribution, (8) the uncorrected Grid-score distribution derived from grid cell population, black dash line represents the corrected threshold for multiple comparison at the 95th percentile of the distribution.

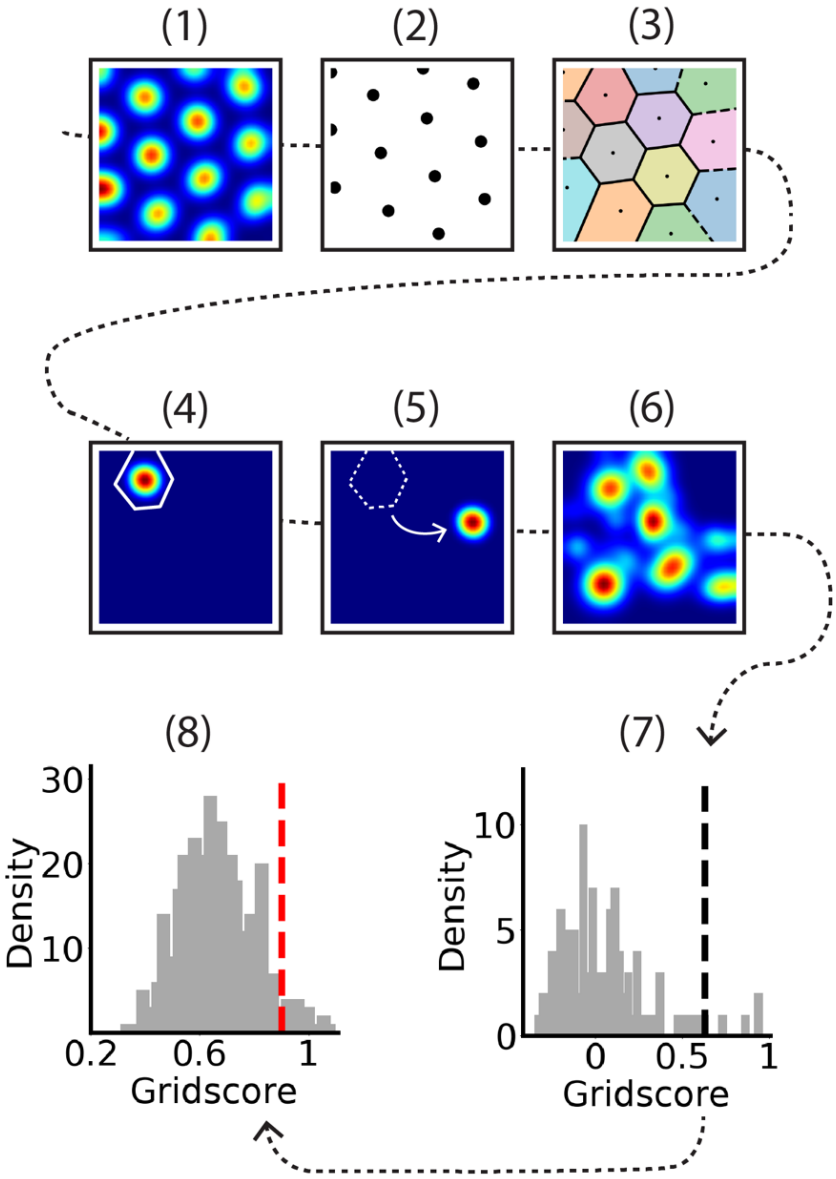

Table S1. Model parameters.

Parameter	Variable	Value
Membrane voltage threshold	η	0
Time constant	τ	10
Weight matrix	W	
Positive peak		0.003
Negative peak		-0.001
Mean		0
Amplitude of planar wave	α	0.333
Grid scales	$\vec{\sigma}$	11-30 pixels (20 samples)
Space size	N	45 pixels

Reference

Ambrose, R. E., Pfeiffer, B. E., & Foster, D. J. (2016). Reverse replay of hippocampal place cells is uniquely modulated by changing reward. Neuron, 91(5), 1124-1136.

Barry, C., & Burgess, N. (2017). To be a Grid Cell: Shuffling procedures for determining "Grid-score". BioRxiv, 230250.

Bauer, U. (2021). Ripser: efficient computation of Vietoris–Rips persistence barcodes. Journal of Applied and Computational Topology, 5(3), 391-423.

Bendor, D., & Wilson, M. A. (2012). Biasing the content of hippocampal replay during sleep. Nature neuroscience, 15(10), 1439-1444.

Burak, Y., & Fiete, I. R. (2009). Accurate path integration in continuous attractor network models of grid cells. PLoS computational biology, 5(2), e1000291.

Barry, C., Ginzberg, L. L., O'Keefe, J., & Burgess, N. (2012). Grid cell firing patterns signal environmental novelty by expansion. Proceedings of the National Academy of Sciences, 109(43), 17687-17692.

Behrens, T. E., Muller, T. H., Whittington, J. C., Mark, S., Baram, A. B., Stachenfeld, K. L., & Kurth-Nelson, Z. (2018). What is a cognitive map? Organizing knowledge for flexible behavior. Neuron, 100(2), 490-509.

Burgess, N., Maguire, E. A., & O'Keefe, J. (2002). The human hippocampus and spatial and episodic memory. Neuron, 35(4), 625-641.

Bonnevie, T., Dunn, B., Fyhn, M., Hafting, T., Derdikman, D., Kubie, J. L., ... & Moser, M. B. (2013). Grid cells require excitatory drive from the hippocampus. Nature neuroscience, 16(3), 309-317.

Buzsáki, G. (2015). Hippocampal sharp wave-ripple: A cognitive biomarker for episodic memory and planning. Hippocampus, 25(10), 1073-1188.

Bush, D., Barry, C., Manson, D., & Burgess, N. (2015). Using grid cells for navigation. Neuron, 87(3), 507-520.

Bicanski, A., & Burgess, N. (2019). A computational model of visual recognition memory via grid cells. Current Biology, 29(6), 979-990.

Bellmund, J. L., Deuker, L., & Doeller, C. F. (2019). Mapping sequence structure in the human lateral entorhinal cortex. elife, 8, e45333.

Bellmund, J. L., De Cothi, W., Ruiter, T. A., Nau, M., Barry, C., & Doeller, C. F. (2020). Deforming the metric of cognitive maps distorts memory. Nature human behaviour, 4(2), 177-188.

Couey, J. J., Witoelar, A., Zhang, S. J., Zheng, K., Ye, J., Dunn, B., ... & Witter, M. P. (2013). Recurrent inhibitory circuitry as a mechanism for grid formation. Nature neuroscience, 16(3), 318-324.

Carr, M. F., Jadhav, S. P., & Frank, L. M. (2011). Hippocampal replay in the awake state: a potential substrate for memory consolidation and retrieval. Nature neuroscience, 14(2), 147-153.

Carr, M. F., Karlsson, M. P., & Frank, L. M. (2012). Transient slow gamma synchrony underlies hippocampal memory replay. Neuron, 75(4), 700-713.

Diba, K., & Buzsáki, G. (2007). Forward and reverse hippocampal place-cell sequences during ripples. Nature neuroscience, 10(10), 1241-1242.

Fiete, I. R., Burak, Y., & Brookings, T. (2008). What grid cells convey about rat location. Journal of Neuroscience, 28(27), 6858-6871.

Fuhs, M. C., & Touretzky, D. S. (2006). A spin glass model of path integration in rat medial entorhinal cortex. Journal of Neuroscience, 26(16), 4266-4276.

Foster, D. J., & Wilson, M. A. (2006). Reverse replay of behavioural sequences in hippocampal place cells during the awake state. Nature, 440(7084), 680-683.

Gardner, R. J., Hermansen, E., Pachitariu, M., Burak, Y., Baas, N. A., Dunn, B. A., ... & Moser, E. I. (2022). Toroidal topology of population activity in grid cells. Nature, 602(7895), 123-128.

Gillespie, A. K., Maya, D. A. A., Denovellis, E. L., Liu, D. F., Kastner, D. B., Coulter, M. E., ... & Frank, L. M. (2021). Hippocampal replay reflects specific past experiences rather than a plan for subsequent choice. Neuron, 109(19), 3149-3163.

Ghrist, R. (2008). Barcodes: the persistent topology of data. Bulletin of the American Mathematical Society, 45(1), 61-75.

Hafting, T., Fyhn, M., Molden, S., Moser, M. B., & Moser, E. I. (2005). Microstructure of a spatial map in the entorhinal cortex. Nature, 436(7052), 801-806.

Hägglund, M., Mørreaunet, M., Moser, M. B., & Moser, E. I. (2019). Grid-cell distortion along geometric borders. Current Biology, 29(6), 1047-1054.

Jacob, P. Y., Capitano, F., Poucet, B., Save, E., & Sargolini, F. (2019). Path integration maintains spatial periodicity of grid cell firing in a 1D circular track. Nature Communications, 10(1), 1-13.

Julian, J. B., Keinath, A. T., Frazzetta, G., & Epstein, R. A. (2018). Human entorhinal cortex represents visual space using a boundary-anchored grid. Nature neuroscience, 21(2), 191-194.

Killian, N. J., & Buffalo, E. A. (2018). Grid cells map the visual world. Nature neuroscience, 21(2), 161-162.

Khona, M., & Fiete, I. R. (2022). Attractor and integrator networks in the brain. Nature Reviews Neuroscience, 1-23.

Kang, L., & Balasubramanian, V. (2019). A geometric attractor mechanism for self-organization of entorhinal grid modules. Elife, 8.

Krupic, J., Burgess, N., & O'Keefe, J. (2012). Neural representations of location composed of spatially periodic bands. Science, 337(6096), 853-857.

Knierim, J. J., & Zhang, K. (2012). Attractor dynamics of spatially correlated neural activity in the limbic system. Annual review of neuroscience, 35, 267-285.

Kurth-Nelson, Z., Behrens, T., Wayne, G., Miller, K., Luettgau, L., Dolan, R., ... & Schwartenbeck, P. (2023). Replay and compositional computation. Neuron.

Liu, Y., Dolan, R. J., Kurth-Nelson, Z., & Behrens, T. E. (2019). Human replay spontaneously reorganizes experience. Cell, 178(3), 640-652.

Liu, Y., Mattar, M. G., Behrens, T. E., Daw, N. D., & Dolan, R. J. (2021). Experience replay is associated with efficient nonlocal learning. Science, 372(6544), eabf1357.

Moser, E. I., Moser, M. B., & McNaughton, B. L. (2017). Spatial representation in the hippocampal formation: a history. Nature neuroscience, 20(11), 1448-1464.

McNaughton, B. L., Battaglia, F. P., Jensen, O., Moser, E. I., & Moser, M. B. (2006). Path integration and the neural basis of the 'cognitive map'. Nature Reviews Neuroscience, 7(8), 663-678.

Mattar, M. G., & Daw, N. D. (2018). Prioritized memory access explains planning and hippocampal replay. Nature neuroscience, 21(11), 1609-1617.

Monsalve-Mercado, M. M., & Leibold, C. (2020). Effect of boundaries on grid cell patterns. Physical Review Research, 2(4), 043137.

Momennejad, I. (2020). Learning structures: predictive representations, replay, and generalization. Current Opinion in Behavioral Sciences, 32, 155-166.

Nau, M., Schröder, T. N., Bellmund, J. L., & Doeller, C. F. (2018). Hexadirectional coding of visual space in human entorhinal cortex. Nature neuroscience, 21(2), 188-190.

Nour, M. M., Liu, Y., Arumuham, A., Kurth-Nelson, Z., & Dolan, R. J. (2021). Impaired neural replay of inferred relationships in schizophrenia. Cell, 184(16), 4315-4328.

Ormond, J., & O'Keefe, J. (2022). Hippocampal place cells have goal-oriented vector fields during navigation. Nature, 607(7920), 741-746.

Pfeiffer, B. E. (2020). The content of hippocampal "replay". Hippocampus, 30(1), 6-18.

Peer, M., Brunec, I. K., Newcombe, N. S., & Epstein, R. A. (2021). Structuring knowledge with cognitive maps and cognitive graphs. Trends in cognitive sciences, 25(1), 37-54.

Rolls, E. T., Stringer, S. M., & Elliot, T. (2006). Entorhinal cortex grid cells can map to hippocampal place cells by competitive learning. Network: Computation in Neural Systems, 17(4), 447-465.

Rihm, J. S., & Rasch, B. (2015). Replay of conditioned stimuli during late REM and stage N2 sleep influences affective tone rather than emotional memory strength. Neurobiology of learning and memory, 122, 142-151.

Rennó-Costa, C., & Tort, A. B. (2017). Place and grid cells in a loop: implications for memory function and spatial coding. Journal of Neuroscience, 37(34), 8062-8076.

Suh, J., Foster, D. J., Davoudi, H., Wilson, M. A., & Tonegawa, S. (2013). Impaired hippocampal ripple-associated replay in a mouse model of schizophrenia. Neuron, 80(2), 484-493.

Schiller, D., Eichenbaum, H., Buffalo, E. A., Davachi, L., Foster, D. J., Leutgeb, S., & Ranganath, C. (2015). Memory and space: towards an understanding of the cognitive map. Journal of Neuroscience, 35(41), 13904-13911.

Strange, B. A., Witter, M. P., Lein, E. S., & Moser, E. I. (2014). Functional organization of the hippocampal longitudinal axis. Nature Reviews Neuroscience, 15(10), 655-669.

Samsonovich, A., & McNaughton, B. L. (1997). Path integration and cognitive mapping in a continuous attractor neural network model. Journal of Neuroscience, 17(15), 5900-5920.

Solstad, T., Moser, E. I., & Einevoll, G. T. (2006). From grid cells to place cells: a mathematical model. Hippocampus, 16(12), 1026-1031.

Sargolini, F., Fyhn, M., Hafting, T., McNaughton, B. L., Witter, M. P., Moser, M. B., & Moser, E. I. (2006). Conjunctive representation of position, direction, and velocity in entorhinal cortex. Science, 312(5774), 758-762.

Shipston-Sharman, O., Solanka, L., & Nolan, M. F. (2016). Continuous attractor network models of grid cell firing based on excitatory–inhibitory interactions. The Journal of physiology, 594(22), 6547-6557.

Schuck, N. W., & Niv, Y. (2019). Sequential replay of nonspatial task states in the human hippocampus. Science, 364(6447), eaaw5181.

Stemmler, M., Mathis, A., & Herz, A. V. (2015). Connecting multiple spatial scales to decode the population activity of grid cells. Science Advances, 1(11), e1500816.

Staudigl, T., Leszczynski, M., Jacobs, J., Sheth, S. A., Schroeder, C. E., Jensen, O., & Doeller, C. F. (2018). Hexadirectional modulation of high-frequency electrophysiological activity in the human anterior medial temporal lobe maps visual space. Current Biology, 28(20), 3325-3329.

Schacter, D. L., Addis, D. R., & Buckner, R. L. (2007). Remembering the past to imagine the future: the prospective brain. Nature reviews neuroscience, 8(9), 657-661.

Stensola, H., Stensola, T., Solstad, T., Frøland, K., Moser, M. B., & Moser, E. I. (2012). The entorhinal grid map is discretized. Nature, 492(7427), 72-78.

Tulving, E., & Markowitsch, H. J. (1998). Episodic and declarative memory: role of the hippocampus. Hippocampus, 8(3), 198-204.

Tolman, E. C. (1948). Cognitive maps in rats and men. Psychological review, 55(4), 189.

Wu, X., & Foster, D. J. (2014). Hippocampal replay captures the unique topological structure of a novel environment. Journal of Neuroscience, 34(19), 6459-6469.

Wilming, N., König, P., König, S., & Buffalo, E. A. (2018). Entorhinal cortex receptive fields are modulated by spatial attention, even without movement. Elife, 7, e31745.

Whittington, J. C., McCaffary, D., Bakermans, J. J., & Behrens, T. E. (2022). How to build a cognitive map. Nature neuroscience, 25(10), 1257-1272.

Yoon, K., Lewallen, S., Kinkhabwala, A. A., Tank, D. W., & Fiete, I. R. (2016). Grid cell responses in 1D environments assessed as slices through a 2D lattice. Neuron, 89(5), 1086-1099.

Yang, L., Zhabotinsky, A. M., & Epstein, I. R. (2004). Stable squares and other oscillatory Turing patterns in a reaction-diffusion model. Physical review letters, 92(19), 198303.

Zhang, S., Xiao, M., & Wang, H. (2020). GPU-accelerated computation of Vietoris-Rips persistence barcodes. arXiv preprint arXiv:2003.07989.